nature geoscience

SUPPLEMENTARY INFORMATION

DOI: 10.1038/NGEO2329

The time-transgressive termination of the African Humid Period

Timothy M. Shanahan, Nicholas P. McKay, Konrad A. Hughen, Jonathan T. Overpeck, Bette Otto-Bliesner, Clifford W. Heil, John King, Christopher A. Scholz, John Peck

1. Supplementary Methods

1.1. Study Area

Lake Bosumtwi is a small (~8 km diameter) but deep (~75 meter) stratified lake occupying a meteorite impact crater in the tropical forest zone of southern Ghana (Fig. S1, S2). The lake is internally draining and isolated from the regional groundwater system, making it exceptionally sensitive to changes in the precipitation-evaporation balance [1-3]. Sheltering of the lake by the surrounding crater walls limits deep mixing of the water column, resulting in permanently anoxic bottom waters and the preservation of fine (mm-scale) laminations, which have been previously demonstrated to be annual in nature [4]. Most of the surrounding catchment is forested, except the flat-lying areas, which have been converted to agriculture (e.g., maize, plantain, cassava) over the last few decades [5].

In 1999 and 2004, a series of freeze cores, piston cores and drill cores were collected from the lake depocenter (Fig. S1)[6]. The freeze cores capture the sediment water interface intact and were visually correlated to the piston cores using marker laminations that could be traced in sediment cores across the central basin [4]. The piston cores are finely (mm-scale) and continuously laminated over their entire length, with the exception of the interval between 2.1 and 3.9 meters, which is organic-rich and contains abundant well-preserved remains of the cyanobacteria Anabaena indicative of eutrophic conditions (Unit S1) [4]. Drill cores collected during the Intercontinental Drilling Program (ICDP) sediment coring expedition to the lake in 2004 provide a nearly continuous 290-

meter long sediment record, which spans the last ca. 1.07 Ma [6]. The present study focuses on the uppermost 10.6 meters of this sediment sequence preserved in the piston cores, which covers the last 25 kyr.

Located in southern Ghana, the climate of Lake Bosumtwi is heavily influenced by the West African monsoon, which draws moisture onshore from the Gulf of Guinea during the months of April-October as the monsoon trough migrates northward with the sun (Fig. S2). In winter the winds reverse, and the climate of southern Ghana is influenced by hot, dry northeasterly monsoon winds, which inhibit precipitation over much of North Africa. Because of its near equatorial (6°N) location and its proximity to the coast, the rainy season is longer and precipitation totals are high near the coast and around Lake Bosumtwi (e.g., 1260 mm yr^{-1}) and decrease with increasing latitude [3].

1.2 Age depth modeling

A radiocarbon chronology for the sediment record is based on Bayesian age-depth modeling of 107 radiocarbon ages on plant macrofossils and bulk organic matter covering the upper 21.4 meters (Fig. S3) [7]. Modeling was performed with the R software package BACON [8] and using the IntCal09 radiocarbon calibration curve [9]. Radiocarbon dates from overlapping cores were correlated using matches from marker laminae and magnetic susceptibility profiles and placed on a standardized depth scale (relative meter composite depth scale – RMCD)[7]. For modeling purposes, BACON uses the prior assumption that ages are in stratigraphic order and that sedimentation rates fall within a designated range and follow a long-tailed distribution. The program models sedimentation rates using a simple gamma autoregressive process and generates posterior age distributions using a self-adjusting Markov Chain Monte Carlo algorithm [10]. The result is a population of possible age-depth models, which reflect the probability distributions associated with the analytical radiocarbon age uncertainties as well as the uncertainties in the calibrated ages.

1.3 Reconstruction of paleolake highstands

The paleolake level history was reconstructed using a combination of radiocarbon dated highstand benches identified above the modern lake level, lowstand terraces

identified in seismic data and sediment cores, and lacustrine muds deposited above the modern lake and preserved on the crater walls (Fig. S4, main text, Fig 2b.; for a more detailed description see [1,11]). Radiocarbon dates on roots from a submerged paleoterrace indicate that the lake was at least 60 meters lower at 16.3 ka [1,12]. However, laminated lacustrine silts 20 meters above the modern lake level indicate that the lake was already substantially deeper than today by 14.5 ka. This recovery was interrupted by a lake level regression between 12.9-11.2 ka, followed by a return to deep lake conditions in the early Holocene. The early Holocene highstand deposited extensive lacustrine silts on the walls of the crater, up to 110 meters above the modern lake, until at least 5.7±0.4 ka [1], though significant undated lacustrine silt accumulations above this date indicate that the high lake stand persisted much later than this. A wave-cut notch in the crater rim indicates that the positive water balance during the early Holocene resulted in the lake overflowing the crater rim [4]. Although the lake level record does not completely constrain the end of the Holocene lake level highstand, a well-dated terrace 15 meters above the modern lake level suggest that it had mostly receded by ca. 2.8-3.5 ka. Submerged terraces, identified in seismic data and confirmed in proxy data suggest that the lake shrank by more than 25 meters below modern lake level at least twice in the last 2 millennia, the most recent of which occurring coincident with the Little Ice Age (1500-1800 AD) [1,13].

Constraints on the timing of the maximum lake level come from radiocarbon dating of a maximum highstand terrace ca. 110 meters above the modern lake surface and cosmogenic surface exposure dating of wavecut bedrock in the overflow spillway at the same elevation. Radiocarbon dates on charcoal from the base of the highstand terrace yield an age of 8.6-9.0 ka, which we interpret as indicating the onset of overflowing conditions [1]. Cosmogenic radiocarbon surface exposure ages on eroded bedrock from the overflow provide an estimate of when water ceased overflowing from the crater. Earlier exposure ages estimates were similar to that obtained from the highstand terrace (9.5±1.5 ka) [1]. However, a revised age estimate using updated cosmogenic ^{14}C production rate estimates and scaling procedures (assuming a spallation production rate of 13.6 atom/gram/yr at sea level and high latitude [14]; and computed with the Cronus calculator [15]), yielded significantly younger ages (5.9±0.9, 6.2±0.9 ka). Together these data suggest

that the lake overflowed for a significant portion of the early Holocene (i.e., between ca. 9.0 and 6.0 ka), consistent with the δD record.

1.4 Stable isotope analysis of leaf waxes

1.4.1 *n*-alkane extraction and separation

1-5 gram sediment samples were freeze dried and solvent extracted using either a Dionex Accelerated Solvent Extraction System or a CEM MARS X Microwave Extraction System with dichloromethane:methanol (9:1; v/v) to obtain a total lipid extract (TLE). The TLE was partitioned into acid and neutral fractions by aminopropyl flash chromatography using 9:1 DCM:MeOH and 2% formic acid in DCM. The neutral fraction concentrated under N_2 and separated into polar and apolar fractions over silica gel with hexane and MeOH. Either urea adduction or molecular sieve was used to remove branched compounds and when needed, Ag^+ chromatography was used to isolate the alkane and alkene fractions prior to stable isotope analysis.

1.4.2 Hydrogen isotope analysis of n-alkanes

Hydrogen isotope analysis of individual *n*-alkanes was performed using an Agilent 6890 gas chromatograph operated in splitless mode and equipped with a DB-5 ms column (30m x 0.25μm x 0.25mm), coupled to a Delta V isotope ratio mass spectrometer via a pyrolysis interface operated at 1430°C. H_3^+ factors were determined daily, and external isotope standards (either the B_2 *n*-alkane or F_8 FAME mix, Indiana University Biogeochemical Laboratories) were measured between every 6 to 8 samples. The external standards had a precision of <±5 ‰. Coinjection of propane during the analysis of the external standards allowed us to determine the isotope value of our propane reference tank and allowed us to use the propane as an internal standard within each unknown sample analysis. Between three and five propane injections were performed during each sample run. Within each run the propane peaks had a precision of <±5 ‰. Most samples were run in either duplicate or triplicate and the standard deviations based on replicate analysis of the same samples was typically <±3 ‰.

1.4.3 Correcting leaf wax hydrogen isotopes for ice volume and vegetation effects

In this study, we interpret changes in δD_{wax} as reflecting changes in the $\delta D_{precipitation}$, which in turn is associated with changes in rainfall amount. On glacial-interglacial timescales there is an additional effect on the δD of precipitation associated with changes in the isotopic composition of source waters due to changes in ice volume. To correct for this effect, we assumed a 1‰ change in $\delta^{18}O$ at the Last Glacial Maximum (LGM; [16,17]. We converted this change in $\delta^{18}O$ to a change in the δD of the glacial ocean assuming that the deuterium excess of the ocean was zero [18,19]. We then developed a time series of δD_{ocean} values spanning the last 20,000 years by scaling these changes to the LR04 benthic oxygen isotope stack [20]. Changes in δD_{ocean} were then subtracted from measured δD_{wax} values to produce a corrected δD_{wax} record ($\delta D_{corr.}$)

Previous studies of modern vegetation have demonstrated that there is a significant negative isotopic fractionation associated with the incorporation of hydrogen into leaf waxes [21]. This offset appears to be significantly different for plants using the C_3 and C_4 photosynthetic pathways [21], leading to a significant influence on δD_{wax} values when vegetation changes are large (as in this study). To address this, we follow a procedure similar to that used by other workers (e.g., [22]) and use the $\delta^{13}C$ values of the terrestrial leaf waxes to adjust the δD_{wax} values for the effect of vegetation type. Assuming that the dominant control on the $\delta^{13}C_{wax}$ signal is the relative proportions of C_3 woody plants and C_4 grasses, we estimate that the proportion of C_4 grasses shifted from ~60% in the deglacial to ~10% in the late Holocene. The magnitude, abruptness and approximate timing of this change are in good agreement with a previously published, lower resolution record of changes in grass pollen from Lake Bosumtwi[23] (% grass pollen shifts from 60% to ~5%), supporting our assumption that the $\delta^{13}C$ signal is predominantly the result of changes in vegetation type. Using these $\delta^{13}C_{wax}$-derived estimates of vegetation changes, we estimate the apparent fractionation factor between the δD_{wax} (for the C_{31} *n*-alkane) and the $\delta D_{precipitation}$($\varepsilon_{wax\text{-}precip.}$) using endmember values reported for grasses (-145±15‰)[24] and tropical forests (-125±5‰)[25] following previous workers[22].

$$\delta \mathrm{D}_{\mathrm{corr.}} = \left[\frac{\delta D_{wax}+1000}{\left(\frac{\varepsilon}{1000}\right)+1}\right] - 1000$$

Because of the large change in $\delta^{13}C$ between the glacial/deglacial period prior to 14.6 ka, and the Holocene, this adjustment significant alters the relative magnitude of the changes in δD_{wax} over the deglaciation. However, it makes relatively little difference in the overall timing or rate of δD changes in the record (Fig. S5).

1.5 Synthesis of paleohydrologic records

To better understand spatiotemporal variations in North African hydroclimate, we synthesized available published records from the literature (Table S1, Fig S6a,b, Fig. S7 animation, main text, Fig. 3). The synthesis draws upon near-shore paleomarine and paleolimnological records based on a wide variety of proxies including stable isotopes ($\delta^{18}O$, $\delta^{13}C$), biological indicators (diatoms, ostracodes, molluscs), stratigraphic dating of paleolacustrine deposits and lithological changes, palynological reconstructions of vegetation changes, and changes in geochemistry. We also include all published δD_{wax} records spanning the time interval of interest and records of changing terrigenous dust fluxes in marine records. All reported uncalibrated radiocarbon ages were calibrated using CALIB7.0[26]. Where possible, we used the interpretations of the datasets as reported in the original manuscripts or in existing synthesis papers e.g.,[27]. Individual site data was plotted using the clockwheel approach used previously for the Asian monsoon system [28]. We excluded data from the non-peer reviewed literature, in which paleohydrologic or vegetation inferences were uncertain, and at sites where significant portions of the AHP were not covered by the reconstructions. To simplify the diagram, we reduced the stable isotope, paleohydrologic and the paleovegetation data to three hydrologic phases: high, intermediate (or transitional) and low. We recognize that these designations may be somewhat subjective, and particularly with the pollen data, may be complicated by other factors such as non-analog vegetation assemblages, local (non-hydrologic) controls on vegetation and anthropogenic modification of the landscape. High values are intervals when the inferred hydrologic balance was at or near the early Holocene maximum. Low values are when the proxy data were interpreted as at or near post-AHP levels.

Intermediate values are when the data fell somewhere in between- not as dry as the post AHP but not as wet as the AHP peak.

To further illustrate the temporal variations in the timing of hydrologic changes, we pooled all of the data for low and high humidity conditions across 5° latitude bands to produce frequency histograms at a 500 yr timestep, following an approach similar to [29] (main text Fig 3, Fig S7a). These histograms serve to summarize the frequency of evidence for wet conditions as a function of time and indicate a time-transgressive shift from wet to dry conditions at the end of the AHP. However, we note that interpretations of these plots should consider the potential complications associated with deflation of the records at the most northernmost sites, which dried out completely. Deflation will preferentially remove the most recent portion of the record with the effect of biasing preservation towards older sediments and could potentially account for some of these apparent time-transgressive features. However, the limited number of continuous records tend to support these reconstructed trends.

We also note that a time-transgressive trend in the timing of the end of the AHP also occurs going from East to West (Fig. S7b). While records from West and Central Africa tend to show a later demise of the AHP, sites to the east (>20° E) occur earlier e.g., 4-5000 cal yr BP. Unlike the records from West Africa, however, the east-west differences in timing cannot be attributed to the truncated nature of the records, providing support the trends apparent in the histograms are robust.

1.6 Changes in the monsoon from the TraCE-21 experiments

To investigate the climate dynamics driving the observed changes in the West African Monsoon, we compared our results to transient simulations of the last 21,000 years performed using the Community Climate System Model, version 3 (CCM3) maintained at NCAR (i.e, the TraCE-21 experiments; www.cgd.ucar.edu/ccr/TraCE/). For most of the comparisons, we chose to examine variables from the ~3.7 x 3.7 degree grid cell centered at 9.8° N, and 0°E. This cell is located about 3° north of Lake Bosumtwi, however, we found it to be most representative of climate at Lake Bosumtwi, primarily because the thermal equator is situated too far North in the TraCE simulation, causing the

grid cell centered at 5.6° N, 0°E to primarily, and unrealistically, respond to changes in Southern Hemisphere insolation.

The TraCE simulation captures the primary pattern of the seasonal migration of the West African rainbelt (Figure S8), however it does not properly simulate the mid-summer dry season on the Guinea Coast. Instead of passing over the Guinea Coast after the May-June rainy season, the monsoon belt *expands* northward into the Sahel while precipitation continues, and even reaches a maximum during August on the Guinea Coast. This effect is enhanced by our choice of grid cell situated North of the lake.

To better understand the climate dynamics underlying the observed and simulated changes in moisture balance at Lake Bosumtwi during the deglaciation, especially with respect to freshwater forcing in the North Atlantic during Heinrich 1 and the Younger Dryas, we examined the behavior of the African and Tropical Easterly Jets during those intervals. Throughout the TraCE-21 experiment, the speed of the upper-level Tropical Easterly Jet, which is associated with the intensity of the West African Monsoon (Nicholson, 2008), is insensitive to freshwater forcing, instead, closely tracking tracks Boreal summer insolation (TEJ; Figures S9). This association is likely due to the role of the Asian Monsoon in modulating TEJ speed. In contrast, the position of the mid-level African Easterly does respond to freshwater forcing in the North Atlantic, shifting southward and intensifying over the Sahel during periods of cool SSTs in the North Atlantic (Figure S10). This behavior has been observed in previous experiments (Mulitza et al., 2008), and the enhanced moisture export is hypothesized to have contributed to decreases in moisture in the region during these events.

In contrast to the deglacial period, simulated precipitation at Lake Bosumtwi does not record the variability observed from the proxy evidence during the Holocene. The lack of a mid-summer dry season in the simulation may explain this data-model mismatch. Focusing on seasonal, rather than annual, precipitation, the peaks in precipitation corresponding to the two rainy seasons at Lake Bosumtwi are observed in the simulation (Fig S11). Precipitation during both the first (MJJ) and second (SO) rainy seasons track local insolation during those months, implicating the role of local insolation on precipitation, and supporting our hypothesis that the late Holocene peak in

precipitation at Lake Bosumtwi, and elsewhere in low-latitude West Africa, was driven in part by an increase in precipitation during the Boreal fall, rather than the summer.

Supplementary References

1 Shanahan, T. M. *et al.* Paleoclimatic variations in West Africa from a record of late Pleistocene and Holocene lake level stands of Lake Bosumtwi, Ghana. *Paleogeogr. Paleoclimatol. Paleoecol.* **242**, 287-302 (2006).

2 Turner, B. F., Gardner, L. R. & Sharp, W. E. The hydrology of Lake Bosumtwi, a climate-sensitive lake in Ghana, West Africa. *Journal of Hydrology* **183**, 243-261 (1996).

3 Shanahan, T. M., Overpeck, J. T., Sharp, W. E., Scholz, C. A. & Arko, J. A. Simulating the response of a closed-basin lake to recent climate changes in tropical West Africa (Lake Bosumtwi, Ghana). *Hydrological Processes* **21**, 1678-1691 (2007).

4 Shanahan, T. M. *et al.* The formation of biogeochemical laminations in Lake Bosumtwi, Ghana, and their usefulness as indicators of past environmental changes. *Journal of Paleolimnology* **40**, 339-355 (2008).

5 Shanahan, T. M. *et al.* Spatial and temporal variability in sedimentological and geochemical properties of sediments from an anoxic crater lake in West Africa: Implications for paleoenvironmental reconstructions. *Paleogeogr. Paleoclimatol. Paleoecol.* **374**, 96-109, (2013).

6 Shanahan, T. M. *et al.* Age models for long lacustrine sediment records using multiple dating approaches - An example from Lake Bosumtwi, Ghana. *Quaternary Geochronology* **15**, 47-60, doi:10.1016/j.quageo.2012.12.001 (2013).

7 Shanahan, T. M. *et al.* Late Quaternary sedimentological and climate changes at Lake Bosumtwi Ghana: New constraints from laminae analysis and radiocarbon age modeling. *Palaeogeography, Palaeoclimatology, Palaeoecology* (2012).

8 Blaauw, M. & Christen, J. Flexible paleoclimate age-depth models using an autoregressive gamma process. *Bayesian Analysis* **6**, 457-474 (2011).

9 Reimer, P. J. *et al.* INTCAL09 and MARINE09 radiocabon age calibration curves, 0-50,000 Years cal BP. *Radiocarbon* **51**, 1111-1150 (2009).

10 Christen, J. & Fox, C. A general purpose sampling algorithm for continuous distributions (the t-walk). *Bayesian Analysis* **4**, 263-282 (2010).

11 Talbot, M. R. & Delibrias, G. A new late-Holocene water-level curve for Lake Bosumtwi, Ghana. *Earth and Planetary Science Letters* **47**, 336-344 (1980).

12 Brooks, K. *et al.* Late-Quaternary lowstands of lake Bosumtwi, Ghana: evidence from high-resolution seismic-reflection and sediment-core data. *Paleogeogr. Paleoclimatol. Paleoecol.* **216**, 235-249 (2005).
13 Shanahan, T. M. *et al.* Atlantic Forcing of Persistent Drought in West Africa. *Science* **324**, 377-380, (2009).
14 Lifton, N. A. *et al.* Addressing solar modulation and long-term uncertainties in scaling secondary cosmic rays for in situ cosmogenic nuclide applications. *Earth and Planetary Science Letters* **239**, 140-161, (2005).
15 Balco, G., Stone, J. O., Lifton, N. A. & Dunai, T. J. A complete and easily accessible means of calculating surface exposure ages or erosion rates from (10)Be and (26)Al measurements. *Quaternary Geochronology* **3**, 174-195, (2008).
16 Schrag, D. P., Hampt, G. & Murray, D. W. Pore fluid constraints on the temperature and oxygen isotopic composition of the glacial ocean. *Science* **272**, 1930-1932, (1996).
17 Shackleton, N. J. The 100,000-year ice-age cycle identified and found to lag temperature, carbon dioxide, and orbital eccentricity. *Science* **289**, 1897-1902, (2000).
18 Tierney, J. E., Russell, J. M., Damste, J. S. S., Huang, Y. & Verschuren, D. Late Quaternary behavior of the East African monsoon and the importance of the Congo Air Boundary. *Quaternary Science Reviews* **30**, 798-807, (2011).
19 Vimeux, F. *et al.* A 420,000 year deuterium excess record from East Antarctica: Information on past changes in the origin of precipitation at Vostok. *Journal of Geophysical Research-Atmospheres* **106**, 31863-31873, (2001).
20 Lisiecki, L. E. & Raymo, M. E. A Pliocene-Pleistocene stack of 57 globally distributed benthic delta O-18 records (vol 20, art no PA1003, 2005). *Paleoceanography* **20**, (2005).
21 Sachse, D. *et al.* Molecular Paleohydrology: Interpreting the Hydrogen-Isotopic Composition of Lipid Biomarkers from Photosynthesizing Organisms. *Annu. Rev. Earth Planet. Sci.* **40**, 221-249 (2012).
22 Collins, J. A. *et al.* Estimating the hydrogen isotopic composition of past precipitation using leaf-waxes from western Africa. *Quaternary Science Reviews* **65**, 88-101 (2013).
23 Maley, J. Late Quaternary climatic changes in the African rain forest: Forest refugia and the major role of sea surface temperature variations. In *Paleoclimatology and Paleometeorology: Modern and Past Patterns of Global Atmospheric Circulation* (eds M. Leinen & M. Sarnthein) 585-616 (Kluwer Academic Publishers, 1989).
24 Smith, F. A., Freeman, K. H. . Influence of physiology and climate on δD of leaf wax n-alkanes from C_3 and C_4 grasses. *Geochimica et Cosmochimica Acta* **70**, 1172-1187 (2006).
25 Polissar, P. J., Freeman, K. H. . Effects of aridity and vegetation on plant-wax δD in modern lake sediments. *Geochimica et Cosmochimica Acta* **74**, 5785-5797. (2010).
26 Stuiver, M., Reimer, P. J., Reimer, R. W. CALIB 5.0. [http://calib.qub.ac.uk/calib/manual/%5D. (2005).
27 Hoelzmann, P. *et al.* in *Past climate variability through Europe and Africa* 219-256 (Springer, 2004).

28 Overpeck, J., Anderson, D., Trumbore, S. & Prell, W. The southwest Indian Monsoon over the last 18 000 years. *Climate Dynamics* **12**, 213-225 (1996).
29 Lezine, A. M., Hely, C., Grenier, C., Braconnot, P. & Krinner, G. Sahara and Sahel vulnerability to climate changes, lessons from Holocene hydrological data. *Quaternary Science Reviews* **30**, 3001-3012, (2011).
30 Huffman, G. J., R.F. Adler, D.T. Bolvin, G. Gu, E.J. Nelk. The TRMM Multi-satellite Precipitation Analysis: Quasi-global, multi-year, combined sensor precipitation estimates at fine scale. *Journal of Hydrometeorlogy* **8**, 38-55 (2007).
31 Schefuß, E., Schouten, S. & Schneider, R. Climatic controls on central African hydrology during the past 20,000 years. *Nature* **437**, 1003-1006 (2005).
32 Niedermeyer, E. M. *et al.* Orbital- and millennial-scale changes in the hydrologic cycle and vegetation in the western African Sahel: insights from individual plant wax δD and δ13C. *Quaternary Science Reviews* **29**, 2996-3005, doi:10.1016/j.quascirev.2010.06.039 (2010).
33 Talbot, M. R. & Johannessen, T. A high resolution paleoclimatic record for the last 27,000 years in tropical West Africa from the carbon and nitrogen isotopic composition of lacustrine organic matter. *Earth and Planetary Science Letters* **110**, 23-37 (1992).
34 Garcin, Y. *et al.* Hydrogen isotope ratios of lacustrine sedimentary n-alkanes as proxies of tropical African hydrology: Insights from a calibration transect across Cameroon. *Geochimica et Cosmochimica Acta* **79**, 106-126, (2012).
35 Gasse, F., Téhet, R., Durand, A., Gibert, E., Fontes, J.C. The arid-humid transition in the Sahara and the Sahel during the last deglaciation. *Nature* **345**, 141-146 (1990).
36 Gasse, F. Diatom-inferred salinity and carbonate oxygen isotopes in Holocene waterbodies of the western Sahara and Sahel (Africa). *Quaternary Science Reviews* **21**, 737-767 (2002).
37 Gilbert, A. M., Conrad, G., De Deckker, P., Fontes, J.C., Gasse, F., Kassir, A. Retour des conditions humides au Tardiglaciaire au Sahara septentrional (Sebkha Mellala, Algerie). *Bulletin de la Société Géologique de France* **6**, 497-504 (1990).
38 Fontes, J. C. *et al.* Freshwater to marine-like environments from Holocene lakes in northern Sahara. *Nature* **317**, 608-610, (1985).
39 Gasse, F., Fontes, J.C., Plaziat, J.C., Carbonnel, P., Kaczmarska, P., De Deckker, P., Soulié-Marsche, I., Callot, Y. Biological remains, geochemistry and stable isotopes for the reconstruction of environmental and hydrological changes in the Holocene lakes from North Sahara. *Palaeogeography, Palaeoclimatology, Palaeoecology* **60**, 1-46 (1987).
40 Kuhlmann, H., Meggers, H., Freudenthal, T. & Wefer, G. The transition of the monsoonal and the N Atlantic climate system off NW Africa during the Holocene. *Geophysical Research Letters* **31**, L22204, (2004).
41 McGee, D., Demenocal, P. B., Winckler, G., Stuut, J. B. W. & Bradtmiller, L. I. The magnitude, timing and abruptness of changes in North African dust deposition over the last 20,000yr. *Earth Planet Sc Lett* **371-372**, 163-176, (2013).
42 deMenocal, P., Ortiz, Joseph, Guilderson, Tom, Sarnthein, Michael. Coherent High- and Low-Latitude Climate Variability During the Holocene Warm Period. *Science* **288**, 2198-2202 (2000).

43 Multiza. Sahel megadroughts triggered by glacial slowdowns of Atlantic meridional overturning. 1-30 (2008).
44 Lezine, A.-M. & Chateauneuf, J.-J. Peat in the "Niayes" of Senegal: depositional environment and Holocene evolution. *Journal of African Earth Sciences (and the Middle East)* **12**, 171-179 (1991).
45 Deynoux, M. *et al.* Stratigraphie séquentielle en milieu désertique. Exemple de l'erg Akchar en Mauritanie occidentale. *Comptes Rendus Académie des Sciences, Paris II* **317**, 1199-1205 (1993).
46 Kocurek, G., Havholm, K. G., Deynoux, M. & Blakey, R. C. Amalgamated accumulations resulting from climatic and eustatic changes, Akchar Erg, Mauritania. *Sedimentology* **38**, 751-772 (1991).
47 Lézine, A.-M. *Paléoenvironnements végétaux d'Afrique nord tropicale depuis 12000 BP*, University Aix-Marseille, (1987).
48 Lézine, A.-M. & Casanova, J. Pollen and hydrological evidence for the interpretation of past climates in tropical West Africa during the Holocene. *Quaternary Science Reviews* **8**, 45-55 (1989).
49 Lézine, A.-M., Casanova, J. & Hillaire-Marcel, C. Across an early Holocene humid phase in western Sahara: Pollen and isotope stratigraphy. *Geology* **18**, 264-267 (1990).
50 Delibrias, G., Petit-Maire, N. & Fabre, J. Ages des dépôts lacustres récents de la région de Taoudenni-Trhaza (Sahara malien). *Comptes Rendus de l'Académie des Sciences, Paris* **299**, 1343-1346 (1984).
51 Fabre, J. & Petit-Maire, N. Holocene climatic evolution at 22–23 N from two palaeolakes in the Taoudenni area (northern Mali). *Palaeogeography, Palaeoclimatology, Palaeoecology* **65**, 133-148 (1988).
52 Petit-Maire, N. Taoudenni basin (Mali), Holocene palaeolimnology and environments. *Würzburger Geographische Arbeiten* **69**, 45-52 (1988).
53 Hillaire-Marcel, C., Riser, J., Rognon, P., Petit-Maire, N., Rosso, J.C., Soulie-Marche, I. Radiocarbon chronology of Holocene hydrologic changes in northeastern Mali. *Quaternary Research* **20**, 145-164 (1983).
54 Petit-Maire, N. Palaeoclimates in the Sahara of Mali. A multidisciplinary Study. *Episodes* **9**, 1-18 (1986).
55 Elenga, H., Maley, J., Vincens, A. & Farrera, I. in *Past climate variability through Europe and Africa* 181-198 (Springer, 2004).
56 Lespez, L. *et al.* High-resolution fluvial records of Holocene environmental changes in the Sahel: the YamE River at Ounjougou (Mali, West Africa). *Quaternary Science Reviews* **30**, 737-756, (2011).
57 Ballouche, A. & Neumann, K. A new contribution to the Holocene vegetation history of the West African Sahel: pollen from Oursi, Burkina Faso and charcoal from three sites in northeast Nigeria. *Vegetation History and Archaeobotany* **4**, 31-39 (1995).
58 Cremaschi, M., di Lernia, S. Holocene climatic changes and cultural dynamics in the Libyan Sahara. *African Archaeological Review* **16**, 211-243 (1999).
59 Cremaschi, M., Zerboni, A. Early to middle holocene landscape exploitation in a drying environment: two case studies compared from the central Sahara (SW Fezzan, Libya). *Comptes Rendus Geoscience* **341**, 689-702 (2009).

60 Baumhauer, R. Palaeolakes of the south central Sahara – problems of palaeoclimatological interpretation. *Hydrobiologia* **214**, 347-357 (1991).
61 Servant, M. Sequences continentales et variations climatiques: evolution du bassin du Tchad au Cenozoique superieur. 573 (Orstom, 1983).
62 Grunert, J., Baumhauser, R., Vökel, J. Lacustrine sediments and Holocene climates in the southern Sahara: the example of paleolakes in the Grand Erg of Bilma (Zoo Baba and Dibelle, eastern Niger). *Journal of African Earth Sciences* **12**, 133-146 (1991).
63 Garba, Z., Durand, A., Lang, J. Enregistrement sédimentaire des variations de la dynamique éolienne pendant la transition Tardiglaciaire/Holocène à la limite Sahara/Sahel (Termit, bassin du lac Tchad). *Zeitschrift für Geomorphologie N.F.* **Suppl. Bd 103**, 159-178 (1996).
64 Waller, M. P., Street-Perrott, F. A. & Wang, H. Holocene vegetation history of the Sahel: pollen, sedimentological and geochemical data from Jikariya Lake, north-eastern Nigeria. *Journal of Biogeography* **34**, 1575-1590, (2007).
65 Salzmann, U., Waller, M. The Holocene vegetational history of the Nigerian Sahel based on multiple pollen profiles. *Review of Palaeobotany and Palynology* **100**, 39-72 (1998).
66 Holmes, J. A., Street-Perrott, F.A., Allen, M.J., Fothergill, P.A., Harkness, D.D., Kroon, D., Perrott, R.A. Holocene palaeolimnology of Kajemarum Oasis, Northern Nigeria: an isotopic study of ostracods, bulk carbonate and organic carbon. *Journal of the Geological Society, London* **154**, 311-319 (1997).
67 Street-Perrott, F. A., Holmes, J.A., Waller, M.P., Allen, M.J., Barber, N.G.H., Fothergill, P.A., Harkness, D.D., Ivanovich, M., Kroon, D., Perrott, R.A. Drought and dust deposition in the West African Sahel: a 5500-year record from Kajemarum Oasis, northeastern Nigeria. *The Holocene* **10**, 293-302 (2000).
68 Gumnior, M., Preusser, F. Late Quaternary river development in the southwest Chad Basin: OSL dating of sediment from the Komadugu palaeofloodplain (northeast Nigeria). *Journal of Quaternary Science* **22**, 709–719 (2007).
69 Hoelzmann, P., Kruse, H.J., Rottinger, F. Precipitation estimates for the eastern Saharan palaeomonsoon based on a water balance model of the West Nubian Palaeolake Basin. *Global and Planetary Change* **26**, 105-120 (2000).
70 Hoelzmann, P., Keding, B., Berke, H., Kröpelin, S., Kruse, H.J. Environmental change and archaeology: lake evolution and human occupation in the Eastern Sahara during the Holocene. *Palaeogeography, Palaeoclimatology, Palaeocology* **169**, 193-217 (2001).
71 Pachur, H. J., Kröpelin, S., Hoelzmann, P., Goschin, M., Altmann, N. Late quaternary fluvio-lacustrine environments of Western Nubian. *Berliner Geowissenschaftliche Abhandlungen (A)* **120**, 203-260 (1990).
72 Pachur, H. J., Hoelzmann, P. Palaeoclimatic implications of Late Quaternary Lacustrine sediments in Western Nubia, Sudan. *Quaternary Research* **36**, 257-276 (1991).
73 Gasse, F. o. & Van Campo, E. Abrupt post-glacial climate events in West Asia and North Africa monsoon domains. *Earth and Planetary Science Letters* **126**, 435-456 (1994).

74 Servant, M. & Servant-Vildary, S. L'environnement quaternaire du bassin du Tchad. *The Sahara and the Nile*, 133-162 (1980).
75 Eggermont, H. *et al.* Aquatic community response in a groundwater-fed desert lake to Holocene desiccation of the Sahara. *Quaternary Science Reviews* **27**, 2411-2425, (2008).
76 Kroepelin, S. *et al.* Climate-driven ecosystem succession in the Sahara: The past 6000 years. *Science* **320**, (2008).
77 Donner, J. The geology of a playa in Farafra, Western Desert of Egypt. *Palaeoecology of Africa* **25**, 121-131 (1998).
78 Donner, J. J., Ashour, M.M., Embabi, N.S., Siiriäinen, A. The Quaternary geology of a playa in Farafra, Western Desert of Egypt. *Annales Academiae Scientiarum Fennicae. Geologica-Geographica* **160**, 49-112 (1999).
79 Hassan, F. A., Barich, B., Mahmoud, M., Hemdan, M.A. Holocene playa deposits of Farafra Oasis, Egypt, and their palaeoclimatic and geoarchaeological significance. *Geoarchaeology: an international journal* **16**, 29-46 (2001).
80 Brookes, I. A. Early Holocene basinal sediments of the Dakhleh oasis region, South central Egypt. *Quaternary Research* **32**, 139-152 (1989).
81 Brookes, I. A. Geomorphology and Quaternary geology of the Dakhla Oasis Region, Egypt. *Quaternary Science Reviews* **12**, 529-552 (1993).
82 Haynes, C. V. in *Prehistory of Arid North Africa* (ed A.E. Close) 69-85 (Southern Methodist University Press, 1987).
83 Haynes, C. V. Geochronology and climat change of the Pleistocene-Holocene transition in the Darb el Arba'in Desert, Eastern Sahara. *Geoarchaeology* **16**, 119-141 (2001).
84 Pachur, H. J., Wünnemann, B. Reconstruction of the palaeoclimate along 30° E in the eastern Sahara during the Pleistocene/ Holocene transition. *Palaeoecology of Africa* **26**, 1-32 (1996).
85 Ritchie, J. C., Haynes, C.V. Holocene vegetation zonation in eastern Sahara. *Nature* **330**, 645-647 (1987).
86 Szabo, B. J., Haynes, C.V., Maxwell, T.A. Ages of Quaternary pluvial episodes determined by uranium-serie and radiocarbon dating of lacustrine deposits of Eastern Sahara. *Palaeogeography, Palaeclimatology, Palaeoecology* **113**, 227-242 (1995).
87 Abell, P. I., Hoelzmann, P., Pachur, H.J. Stable isotopes ratios of gastropod shells and carbonate sediments of NW Sudan ans palaeoclimatic indicators. *Palaeoecology of Africa* **26**, 33-52 (1996).
88 Abell, P. I., Hoelzmann, P. Holocene paleoclimates in northwestern Sudan: stable isotope studies on molluscs. *Global and Planetary Change* **26**, 1-12 (2000).
89 Ritchie, J. C., Eyles, C.H., Haynes, C.V. Sediment and pollen evidence for an early to mid-Holocene humid period in the eastern Sahara. *Nature* **314**, 352-355 (1985).
90 Hoelzmann, P., Schwab, A., Robers, N., Cooper, P., Burgess, A. Hydrological response of an east-Saharan palaeolake (NW Sudan) to early-Holocene climate. *The Holocene* **20**, 537-549 (2010).
91 Pachur, H. J., Hoelzmann, P. Late Quaternary palaeoecology and palaeoclimates of the eastern Sahara. *Journal of African Earth Sciences* **30**, 929-939 (2000).

92 Bubenzer, O., Besler, H., Hilgers, A. Filling the gap: OSL data expanding 14C chronologies of Late Quaternary environmental change in the Libyan Desert. *Quaternary International* **175**, 41–52 (2007).
93 Pachur, H. J., Röper, H.P. The libyan (Western) desert and northern Sudan during the late Pleistocene and holocene *Berliner Geowissenschaftliche Abhandlungen (A)* **50**, 249-284 (1984).
94 Ayliffe, D., Williams, M.A.J., Sheldon, F. Stable isotope and ocygen isotopic composition of early-Holocene gastropods from Wadi Mansurab, north-central Sudan. *The Holocene* **6**, 157-169 (1996).
95 Williams, M. A. J., Adamson, D.A. in *The Sahara and the Nile* (ed M.A.J. Williams, Faure, H.) 281-304 (Balkema, 1981).
96 Cremaschi, M., Zerboni, A., Spötl, C., Felleti, F. The calcareous tufa in the Tadrart Acacus Mt. (SW Fezzan, Lybia). An early holocene palaeoclimate archive in the central sahara. *Palaeogeography, Palaeoclimatology, Palaeoecology* **287**, 81-94 (2010).
97 Barker, P., Telford, R., Gasse, F. & Thevenon, F. Late Pleistocene and Holocene palaeohydrology of Lake Rukwa, Tanzania, inferred from diatom analysis. *Palaeogeography, Palaeoclimatology, Palaeoecology* **187**, 295-305 (2002).
98 Barker, P., Williamson, D., Gasse, F. & Gibert, E. Climatic and volcanic forcing revealed in a 50,000-year diatom record from Lake Massoko, Tanzania. *Quaternary Research* **60**, 368-376 (2003).
99 Costa, K., Russell, J., Konecky, B. & Lamb, H. Isotopic reconstruction of the African Humid Period and Congo Air Boundary migration at Lake Tana, Ethiopia. *Quaternary Science Reviews* **83**, 58-67, doi:10.1016/j.quascirev.2013.10.031 (2014).
100 Gasse, F. Hydrological changes in the African tropics since the Last Glacial Maximum. *Quaternary Science Reviews* **19**, 189-211 (2000).
101 Gasse, F., Rognon, P. & Street, F. Quaternary history of the Afar and Ethiopian Rift lakes. *The Sahara and the Nile (MAJ Williams and H. Faure, Editors).* . 361-400 (1980).
102 Chalié, F. & Gasse, F. Late Glacial-Holocene diatom record of water chemistry and lake level change from the tropical East African Rift Lake Abiyata (Ethiopia). *Palaeogeography, Palaeoclimatology, Palaeoecology* **187**, 259-283 (2002).
103 Tierney, J. E. & deMenocal, P. B. Abrupt shifts in Horn of Africa hydroclimate since the Last Glacial Maximum. *Science Express* **published online October 10 2013** (2013).
104 Jung, S., Davies, G., Ganssen, G. & Kroon, D. Stepwise Holocene aridification in NE Africa deduced from dust-borne radiogenic isotope records. *Earth and Planetary Science Letters* **221**, 27-37, (2004).
105 Benvenuti, M. *et al.* The Ziway-Shala lake basin (Main Ethiopian rift, Ethiopia): a revision of basin evolution with special reference to the Late Quaternary. *Journal of African Earth Sciences* **35**, 247-269 (2002).
106 Gasse, E. & Street, F. Late Quaternary lake-level fluctuations and environments of the northern Rift Valley and Afar region (Ethiopia and Djibouti). *Palaeogeography, Palaeoclimatology, Palaeoecology* **24**, 279-325 (1978).

107 Gillespie, R., Street-Perrott, F. A. & Switsur, R. Post-glacial arid episodes in Ethiopia have implications for climate prediction. *Nature* **306**, 680-683 (1983).
108 Lamb, A., Leng, M., Lamb, H. & Mohammed, M. A 9000-year oxygen and carbon isotope record of hydrological change in a small Ethiopian crater lake. *Holocene* **10**, 167-177 (2000).
109 Jolly, D., Bonnefille, R. & Roux, M. Numerical interpretation of a high resolution Holocene pollen record from Burundi. *Palaeogeography, Palaeoclimatology, Palaeoecology* **109**, 357-370 (1994).
110 Aucour, A., Bonnefille, R. & Hillaire-Marcel, C. Sources and accumulation rates of organic carbon in an equatorial peat bog (Burundi, East Africa) during the Holocene: carbon isotope constraints. *Paleogeogr. Paleoclimatol. Paleoecol.* **150**, 179-189 (1999).
111 Bonnefille, R. *et al.* Glacial/interglacial record from intertropical Africa, high resolution pollen and carbon data at Rusaka, Burundi. *Quaternary Science Reviews* **14**, 917-936 (1995).
112 Taylor, D. Late Quaternary pollen records from two Ugandan mires: Evidence for environmental change in the Rukiga Highlands of southwest Uganda. *Palaeogeography, Palaeoclimatology, Palaeoecology* **80**, 283-300 (1990).
113 Beuning, K. & Russell, J. Vegetation and sedimentation in the Lake Edward Basin, Uganda-Congo during the late Pleistocene and early Holocene. *Journal of Paleolimnology* **32**, 1-18 (2004).
114 Owen, R., Barthelme, J., Renaut, R. & Vincens, A. Palaeolimnology and archaeology of Holocene deposits north-east of Lake Turkana, Kenya. (1982).
115 Beuning, K., Kelts, K., Russell, J. & Wolfe, B. Reassessment of Lake Victoria - Upper Nile River paleohydrology from oxygen isotope records of lake-sediment cellulose. *Geology* **30**, 559-562 (2002).
116 Stager, J., Mayewski, P. & Meeker, L. Cooling cycles, Heinrich event 1, and the desiccation of Lake Victoria. *Paleogeogr. Paleoclimatol. Paleoecol.* **183**, 169-178 (2002).
117 Street-Perrott, F. & Perrott, R. Abrupt climate fluctuations in the tropics: the influence of Atlantic Ocean circulation. *Nature* **343**, 607-612 (1990).
118 Tierney, J. *et al.* Northern Hemisphere controls on tropical southeast African climate during the past 60,000 years. *Science* **322**, 252 (2008).
119 Stager, J. Environmental changes at Lake Cheshi, Zambia since 40,000 years BP. *Quaternary research (USA)* (1988).
120 Salzmann, U. Are modern savannas degraded forests ? - A Holocene pollen record from the Sudanian vegetation zone of NE Nigeria. *Vegetation history and archaeobotany* **9**, 1-15 (2000).
121 Salzmann, U., Hoelzmann, P. & Morczinek, I. Late Quaternary climate and vegetation of the Sudanian zone of northeast Nigeria. *Quaternary Research* **58**, 73-83 (2002).
122 Baumhauer, R., Schulz, E. & Pomel, S. in *Paleoecology of Quaternary Drylands* 31-45 (Springer, 2004).
123 Salzmann, U. & Hoelzmann, P. The Dahomey Gap: an abrupt climatically induced rain forest fragmentation in West Africa during the late Holocene. *Holocene* **15**, 190-199, (2005).

124 Tossou, M. G., Akoegninou, A., Ballouche, A., Sowunmi, M. A. & Akpagana, K. The history of the mangrove vegetation in Benin during the Holocene: A palynological study. *Journal of African Earth Sciences* **52**, 167-174, (2008).
125 Sowunmi, M. A. in *Past climate variability through Europe and Africa* 199-218 (Springer, 2004).
126 Fredoux, A. Evolution de la vegetation dans le delta de l'Agneby (Cote d'Ivoire). *Travaux et documents de geographie tropicale*, 117-134 (1983).
127 Giresse, P., Maley, J. & Brenac, P. Late Quaternary palaeoenvironments in the Lake Barombi Mbo (West Cameroon) deduced from pollen and carbon isotopes of organic matter. *Paleogeogr. Paleoclimatol. Paleoecol.* **107**, 65-78 (1994).
128 Lebamba, J., Vincens, A. & Maley, J. Pollen, vegetation change and climate at Lake Barombi Mbo (Cameroon) during the last ca. 33 000 cal yr BP: a numerical approach. *Climate of the Past* **8**, 59-78, (2012).
129 Maley, J. The African rain forest vegetation and paleoenvironments during the late Quaternary. *Climatic Change* **19**, 79-98 (1991).
130 Weldeab, S., Lea, D. W., Schneider, R. R. & Andersen, N. 155,000 Years of West African Monsoon and Ocean Thermal Evolution. *Science* **316**, 1303-1307, (2007).
131 Lézine, A. Timing of vegetation changes at the end of the Holocene Humid Period in desert areas at the northern edge of the Atlantic and Indian monsoon systems. *Comptes rendus-Géoscience* **341**, 750-759 (2009).
132 Vincens, A. *et al.* Forest response to climate changes in Atlantic Equatorial Africa during the last 4000 years BP and inheritance on the modern landscapes. *Journal of Biogeography* **26**, 879-885 (1999).
133 Zogning, A., Giresse, P., Maley, J. & Gadel, F. o. The Late Holocene palaeoenvironment in the Lake Njupi area, west Cameroon: implications regarding the history of Lake Nyos. *Journal of African Earth Sciences* **24**, 285-300 (1997).
134 Kadomura, H. in *Savannization Processes in Tropical Africa II* (ed H. Kadomura, Kiyonaga, J.) 47–85 (Tokyo Metropolitan University, 1994).
135 Moeyersons, J. Geomorphological processes and their paleoenvironmental significance at the Shum Laka cave (Bamenda, western Cameroon). *Palaeogeography, Palaeoclimatology, Palaeoecology* **133**, 103-116 (1997).
136 Tamura, T. Late Quaternary landscape evolution in the west Cameroon Highlands and the Adamaoua Plateau. *Paysages Quaternaires de L,ÄôAfrique Centrale Atlantique. Paris: Editions de l,ÄôOrstom*, 298-313 (1990).
137 Nguetsop, V. *et al.* Past environmental and climatic changes during the last 7200 cal yr BP in Adamawa plateau (Northern-Cameroun) based on fossil diatoms and sedimentary carbon isotopic records from Lake Mbalang. *Climate of the Past* **7**, 1371-1393 (2011).
138 Vincens, A., Buchet, G. & Servant, M. Vegetation response to the "African Humid Period" termination in central Cameroon (7 N)- new polen insight from Lake Mbalang. *Climate of the Past* **6**, 281-294 (2010).
139 Giresse, P., Maley, J. & Kossoni, A. Sedimentary environmental changes and millennial climatic variability in a tropical shallow lake (Lake Ossa, Cameroon) during the Holocene. *Paleogeogr. Paleoclimatol. Paleoecol.* **218**, 257-285 (2005).

140 Reynaud-Farrera, I., Maley, J. & Wirrmann, D. Végétation et climat dans les forêts du Sud-Ouest Cameroun depuis 4770 ans BP: analyse pollinique des sédiments du Lac Ossa. *Comptes Acad Sci Paris* **322**, 749-755 (1996).
141 Ngomanda, A., K. Neumann, A. Schweizer, J. Maley. Seasonality change and the third millennium BP rainforest crisis in Central Africa: a high resolution pollen profile from Nyabessan, southern Cameroon. *Quaternary Research* **71**, 307-318 (2009).
142 Brncic, T. M., Willis, K. J., Harris, D. J. & Washington, R. Culture or climate? The relative influences of past processes on the composition of the lowland Congo rainforest. *Philos T R Soc B* **362**, 229-242, (2007).
143 Brncic, T. M., Willis, K. J., Harris, D. J., Telfer, M. W. & Bailey, R. M. Fire and climate change impacts on lowland forest composition in northern Congo during the last 2580 years from palaeoecological analyses of a seasonally flooded swamp. *The Holocene* **19**, 79-89 (2009).
144 Laraque, A. *et al.* Reconnaissance scientifique du lac Télé (Nord-Congo) — Premiers résultats et interprétations. *Comptes Rendus de l'Académie des Sciences - Series IIA - Earth and Planetary Science* **325**, 49-56 (1997).
145 Ngomanda, A. *et al.* Vegetation changes during the past 1300 years in western equatorial Africa: a high-resolution pollen record from Lake Kamalete, Lope Reserve, Central Gabon. *Holocene* **15**, 1021-1031, (2005).
146 Elenga, H. *Végétation et climat du Congo depuis 24 000 ans B.P. : analyse palynologique de séquences sédimentaires du Pays Bateke et du littoral*, Université de Droit d'Economie et des Sciences d'Aix-Marseille 3, (1992).
147 Elenga, H. *et al.* Diagramme pollinique holocène du lac Kitina (Congo): mise en évidence de changements paléobotaniques et paléoclimatiques dans le massif forestier du Mayombe. *Compte Rendu de l'Académie des Sciences* **323**, 403-410 (1996).
148 Vincens, A., Schwartz, D., Bertaux, J., Elenga, H. & de Namur, C. Late Holocene climatic changes in western equatorial Africa inferred from pollen from Lake Sinnda, southern Congo. *Quaternary Research* **50**, 34-45 (1998).
149 Elenga, H. *et al.* Le marais estuarien de la Songolo (Sud Congo) a l'Holocene moyen et recent. *Bulletin de la Société Géologique de France* **172**, 359-366 (2001).
150 Elenga, H., Schwartz, D. & Vincens, A. Pollen evidence of late Quaternary vegetation and inferred climate changes in Congo. *Palaeogeography, Palaeoclimatology, Palaeoecology* **109**, 345-356 (1994).

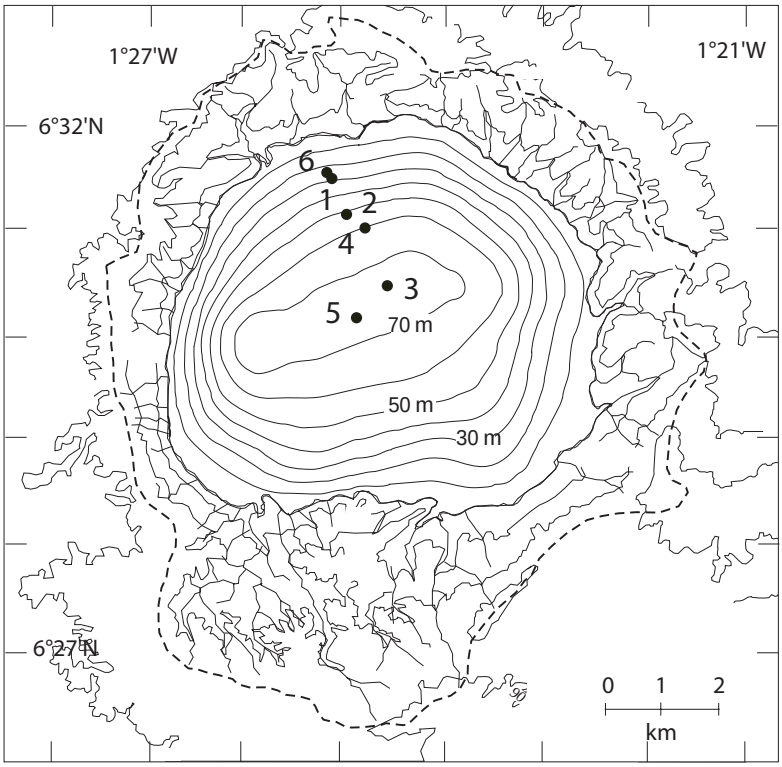

Figure S1. Bathymetric map of the Lake Bosumtwi impact crater. Circles indicate the locations of coring sites used in this study[1]

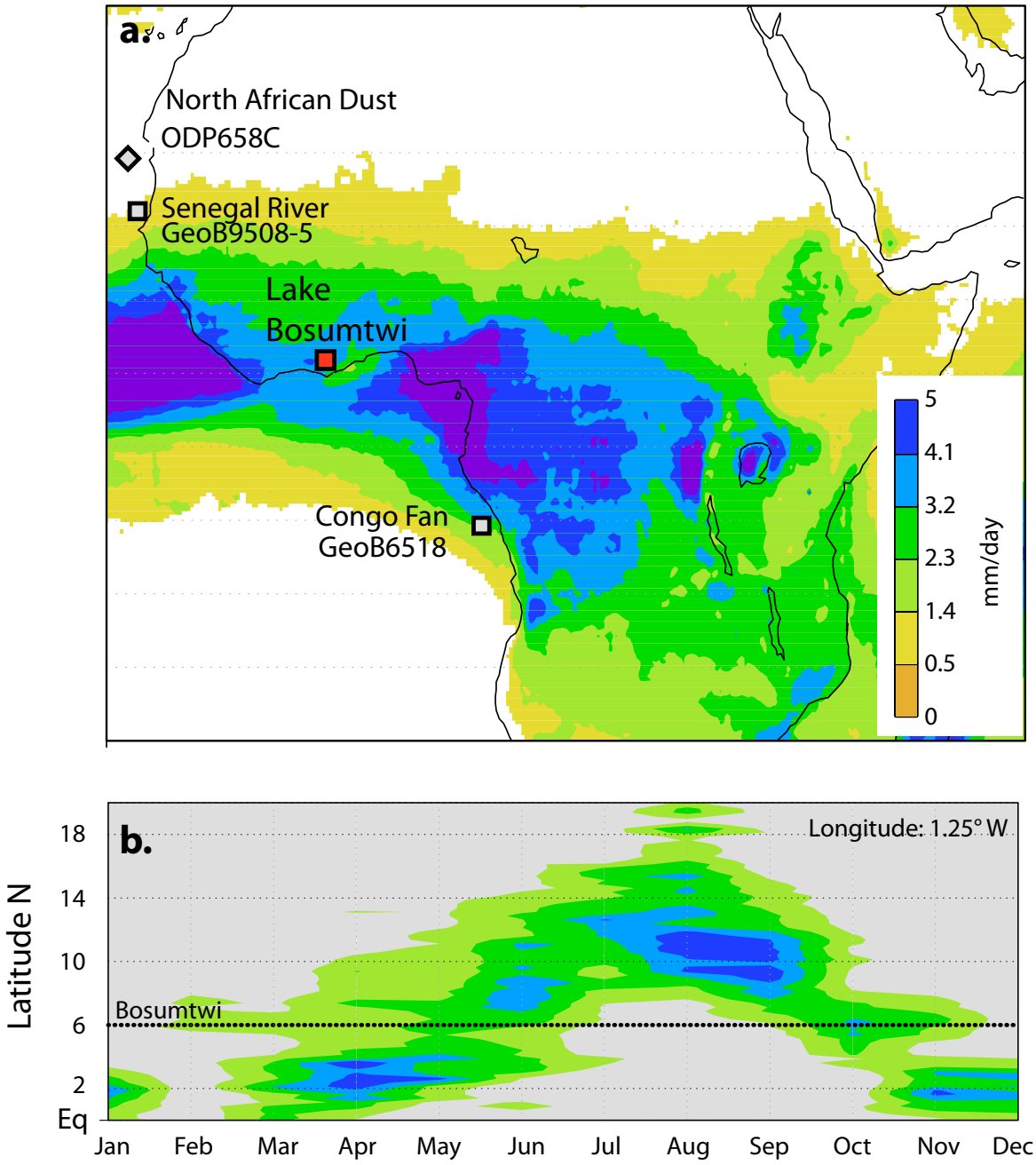

Figure S2. Study locations and precipitation over North Africa. **a.** Mean annual precipitation (mm/day) for the period between 1998-2010 from the Tropical Rainfall Measuring Mission (TRMM) v. 6 [30]. Diamond, site showing an abrupt mid-Holocene termination of the AHP: ODP658c(20°45'N, 18°35'W).[42]. Squares, sites showing a two-stage collapse of the AHP: Red square, study area, Lake Bosumtwi (6°30'N, 1°25'W), Congo River delta core GeoB6518-1 (5°35.5'S, 11°13.3'E) [31], Senegal River core GeoB9508-S (15°29.9'N, 17°56.88'W)[32]. **b.** Hovmöller diagram of the seasonal change in precipitation as a function of latitude at the longitude of Lake Bosumtwi (1°25'W) for 2003 from the Tropical Rainfall Measuring Mission (TRMM) v. 6 dataset.

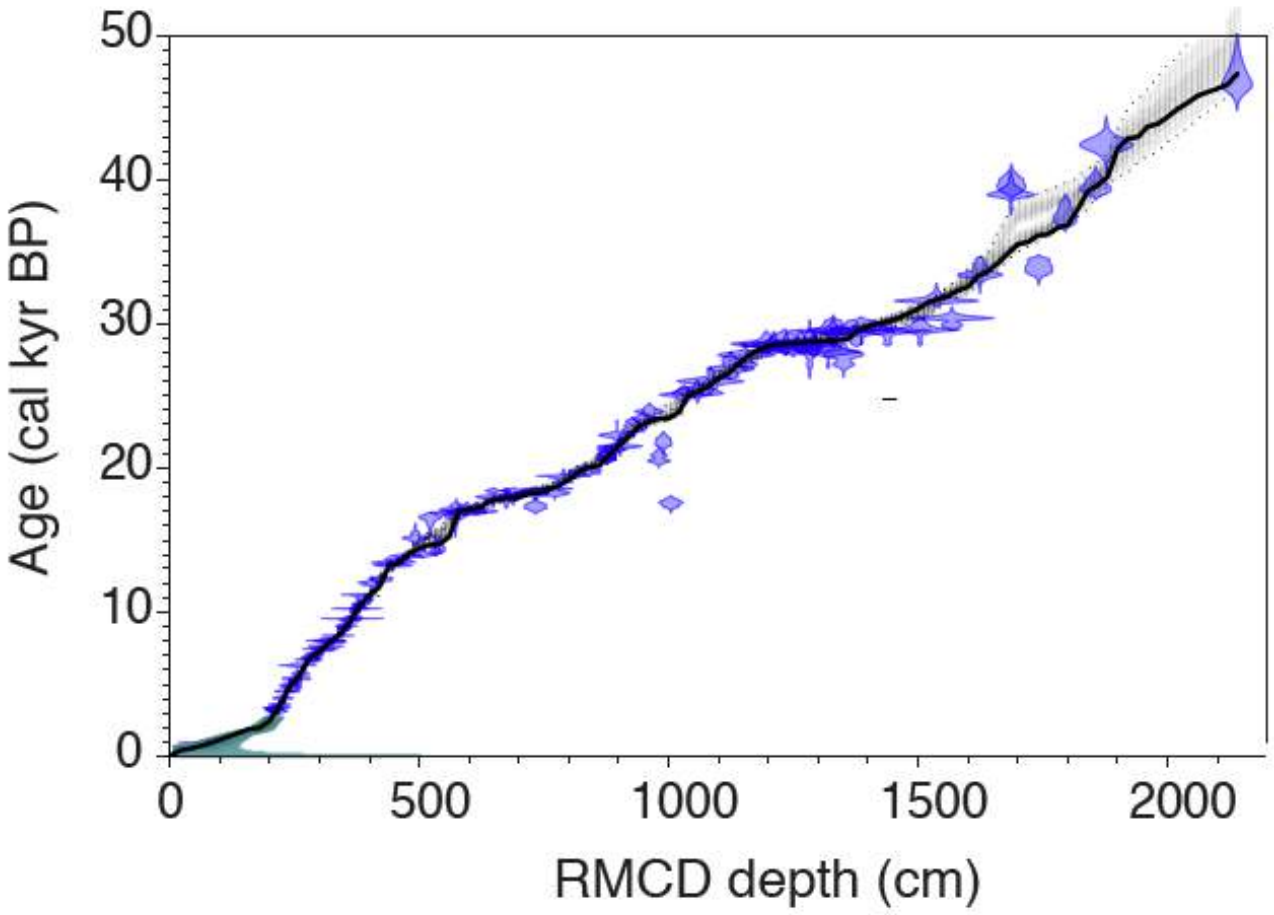

Figure S3. Age depth model for the composite Lake Bosumtwi sediment record (in RMCD standardized depth). Symbols indicate calibrated age distributions for individual radiocarbon ages. The solid black line indicates the optimal age model determined using the bayesian age-depth modeling software BACON[8]. Redrawn from [7].

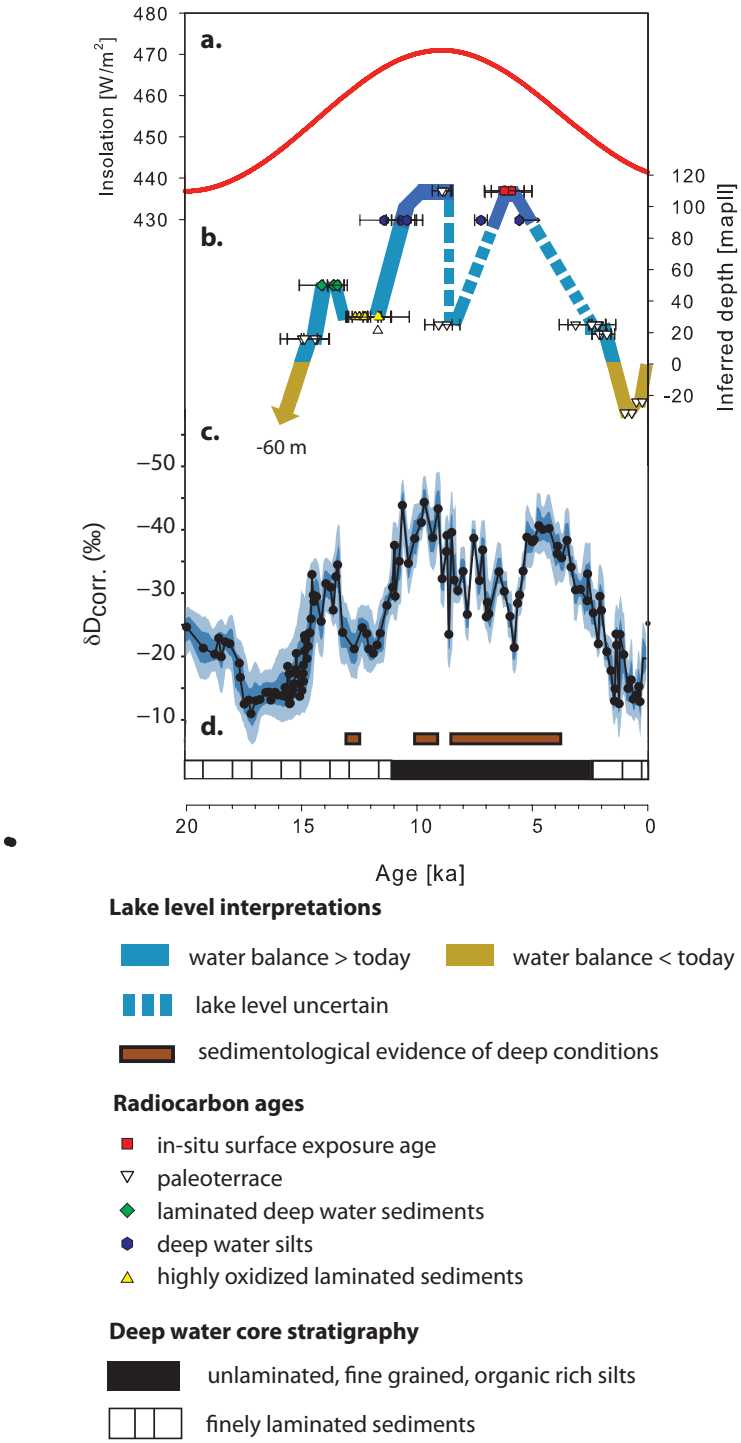

Figure S4. Comparison between leaf wax isotopes and paleolake level reconstruction for Lake Bosumtwi. a. Summer (June-August) insolation changes at 6.5°N. b. Changes in lake level reconstructed from radiocarbon dated terraces and lacustrine silts preserved on the crater walls and identified below the modern lake level. Data was synthesized from previous workers [1,11,12] and revised using new in-situ ^{14}C production rates[14]. c. Hydrogen isotope composition of C_{31} n-alkanes adjusted for changes in vegetation (grey) and vegetation and ice volume (black) (SOM 1.4.3) indicating changes in precipitation. Shading reflects 68% (dark) and 95% (light) uncertainties in the reconstruction, based on analytical and age model errors. d. Idealized core stratigraphy showing the time interval of unit S1, which is organic-rich, unlaminated and dominated by the remains of nitrogen fixing blue green algae indicative of eutrophic conditions[33].

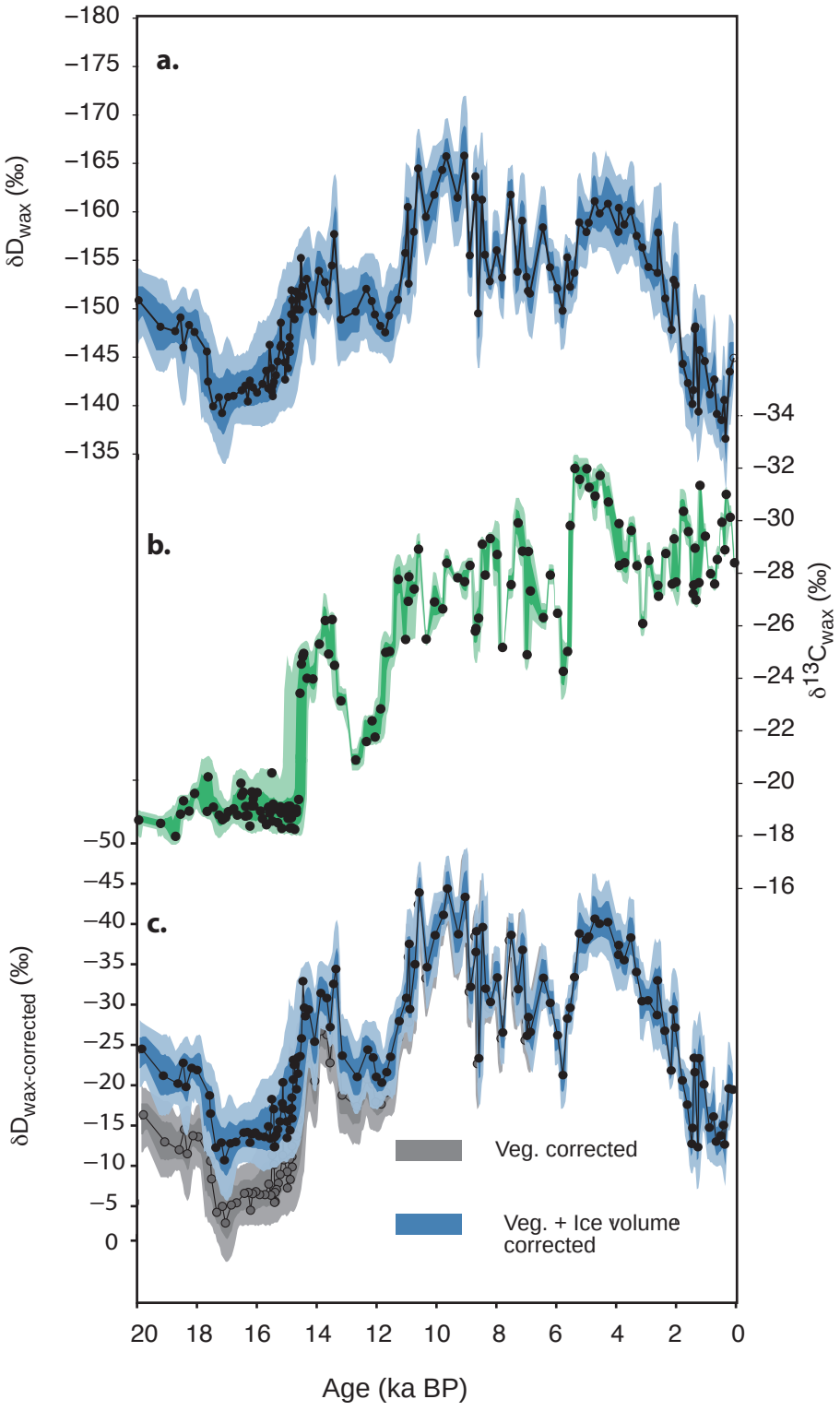

Figure S5. Correction of the δD_{wax} precipitation record for changes in ice volume and vegetation. **a.** Measured δD_{wax} values for the C_{31} n-alkanes in Lake Bosumtwi. **b.** Measured $\delta^{13}C_{wax}$ for the C_{31} n-alkanes. **c.** A comparison between the δD_{wax} record after correction for the influence of vegetation type on apparent fractionation between leaf wax and source water (grey) and after a correction for changes in the isotopic composition of source water due to ice volume (blue).

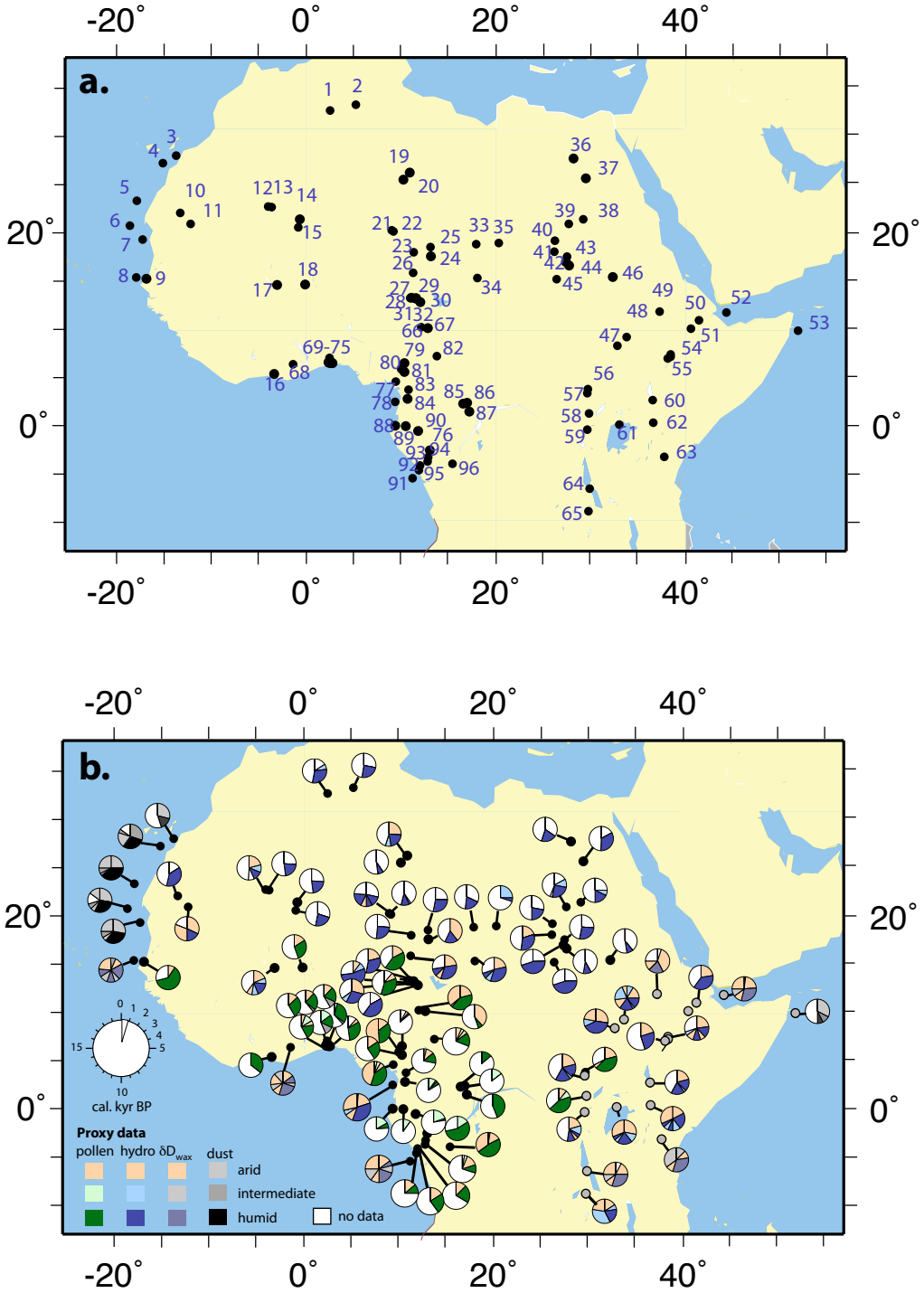

Figure S6. **a.** Sites used in the reconstruction of past hydrological changes across North Africa. See Table S1 for reference number locations. **b.** Clock wheel diagrams synthesizing the evolution of reconstructed changes in hydrology over the last 20,000 years from the published literature. Colors indicate paleohydrologic or paleovegetation conditions; white indicates no data at a given site. Sites with grey symbols are designated here as East Africa and are excluded from the histograms in Fig. S7a. See SOM sec. 1.5 and SOM Table S1 for details and references on individual records.

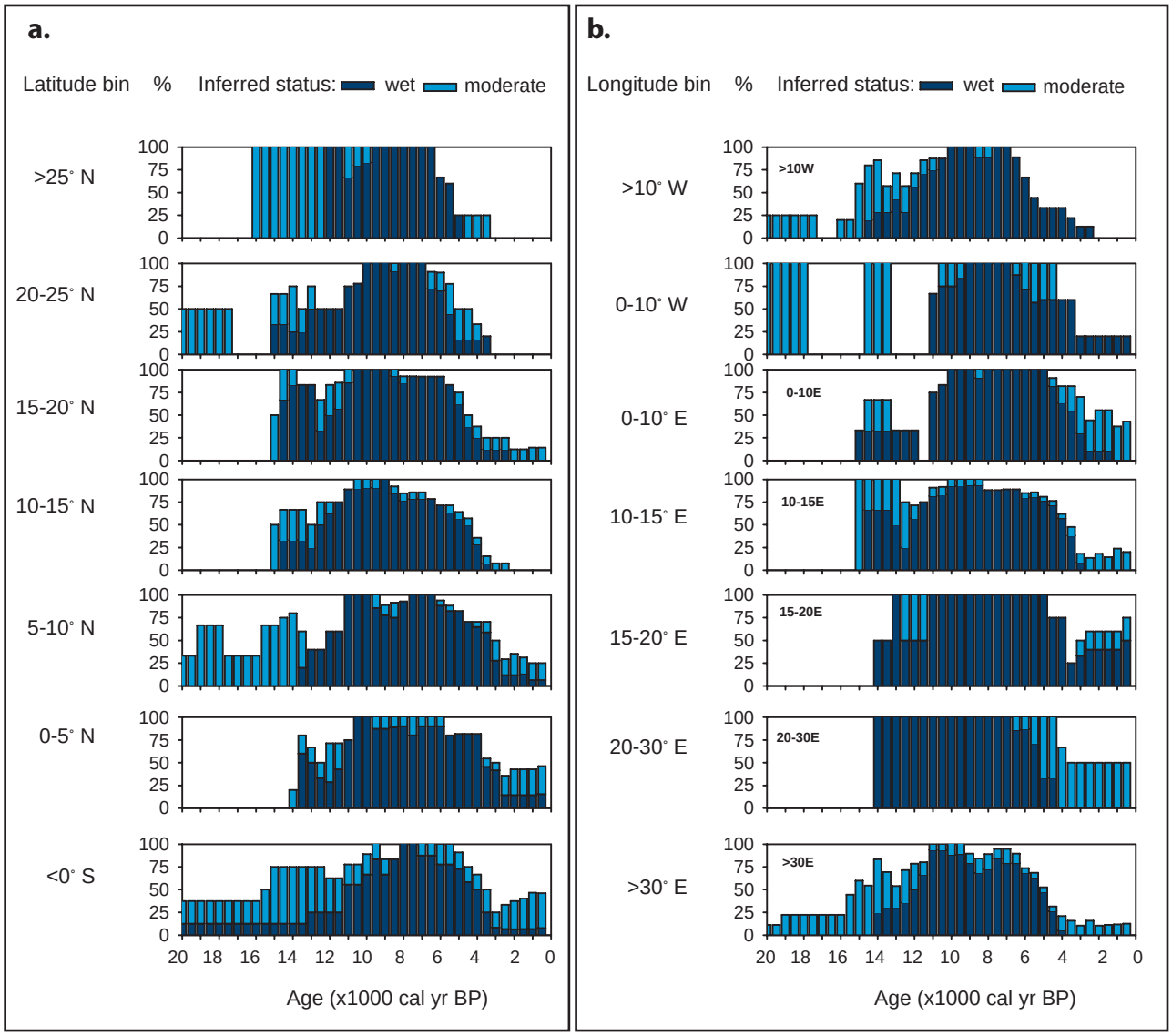

Figure S7. Histograms of wet conditions during the AHP across North Africa. **a.** Same as in main text Figure 3 but with the sites from East Africa excluded. **b.** Histograms in longitudinal bins going from west to east across the study area. Dark blue: maximum wet conditions. Light blue: moderately wet conditions.

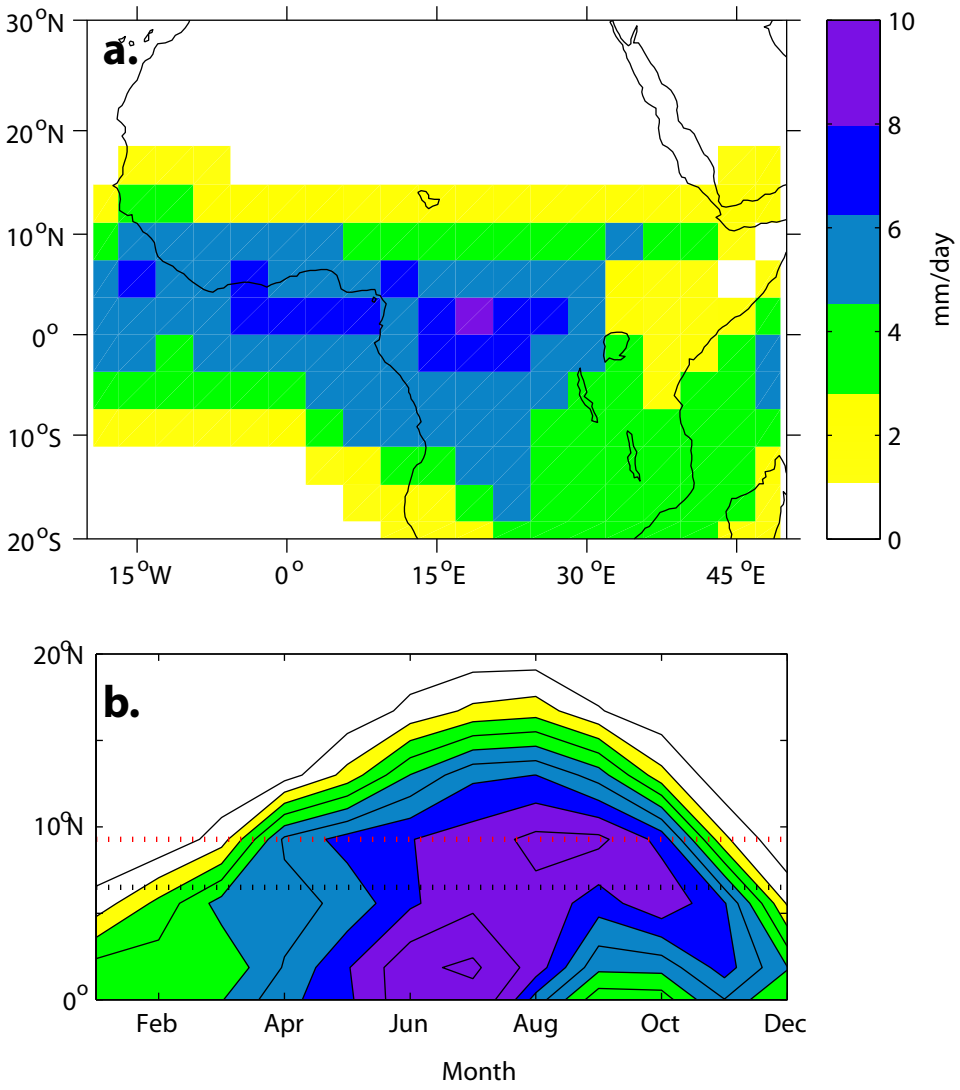

Figure S8. Model simulation of precipitation seasonality over West Africa. **a.**Simulated mean daily precipitation over tropical and subtropical Africa during the most recent 1000 years of the TraCE-21 simulations (991 – 1990 AD). **b.** Latitudinal progression of summer monsoon precipitation in West Africa as a function of month, at 0°E. The latitude of Lake Bosumtwi (6.5°N) is shown by the black dashed line; the mid-point latitude (9.8°N) of the grid cell used for comparison in this study shown by the red dashed line.

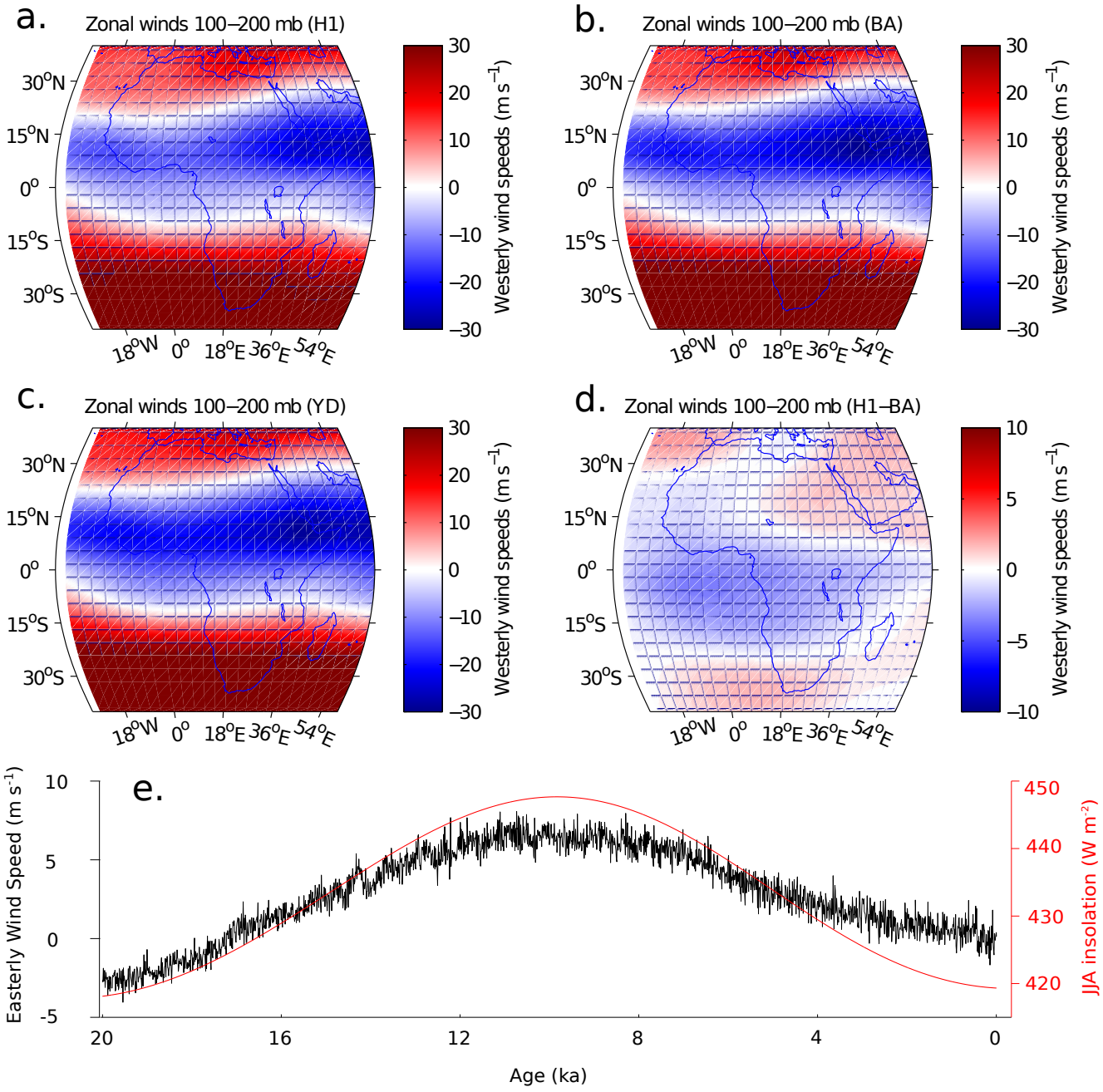

Figure S9. Speed and velocity of the Tropical Easterly Jet for June-August (JJA) during the deglaciation. A-D) Simulated zonal wind speeds, averaged over 100-200 mb, for A) Heinrich 1 (17 to 14.7 ka), B) Bolling-Allerod (14.6 to 13 ka) C) Younger Dryas (12.9 to 11.5 ka) and D) The difference between A and B. E) Simulated average JJA zonal wind speed over the past 20 kyr, averaged over 0 to 15°N, -20 to 20°E, and 100 to 200 mb shown in black, with average JJA insolation at 6.5 N in red.

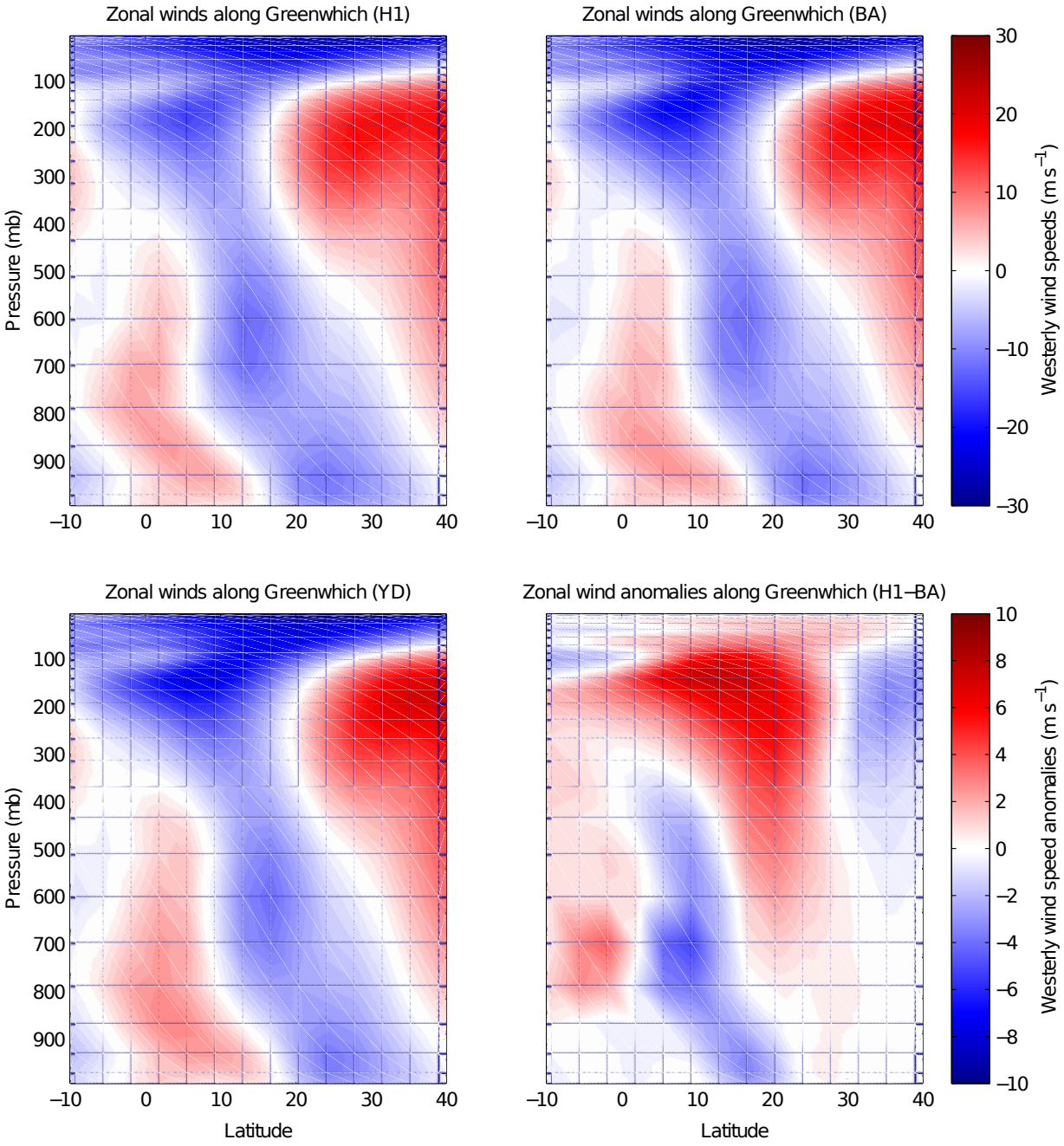

Figure S10. Simulated zonal wind speeds between 10°S and 40°N along the Greenwhich Meridian, for Heinrich 1 (H1; 17 to 14.7 ka), the Bolling-Allerod (BA; 14.6 to 13 ka), the Younger Dryas (YD; 12.9 to 11.5 ka) and the difference between H1 and BA.

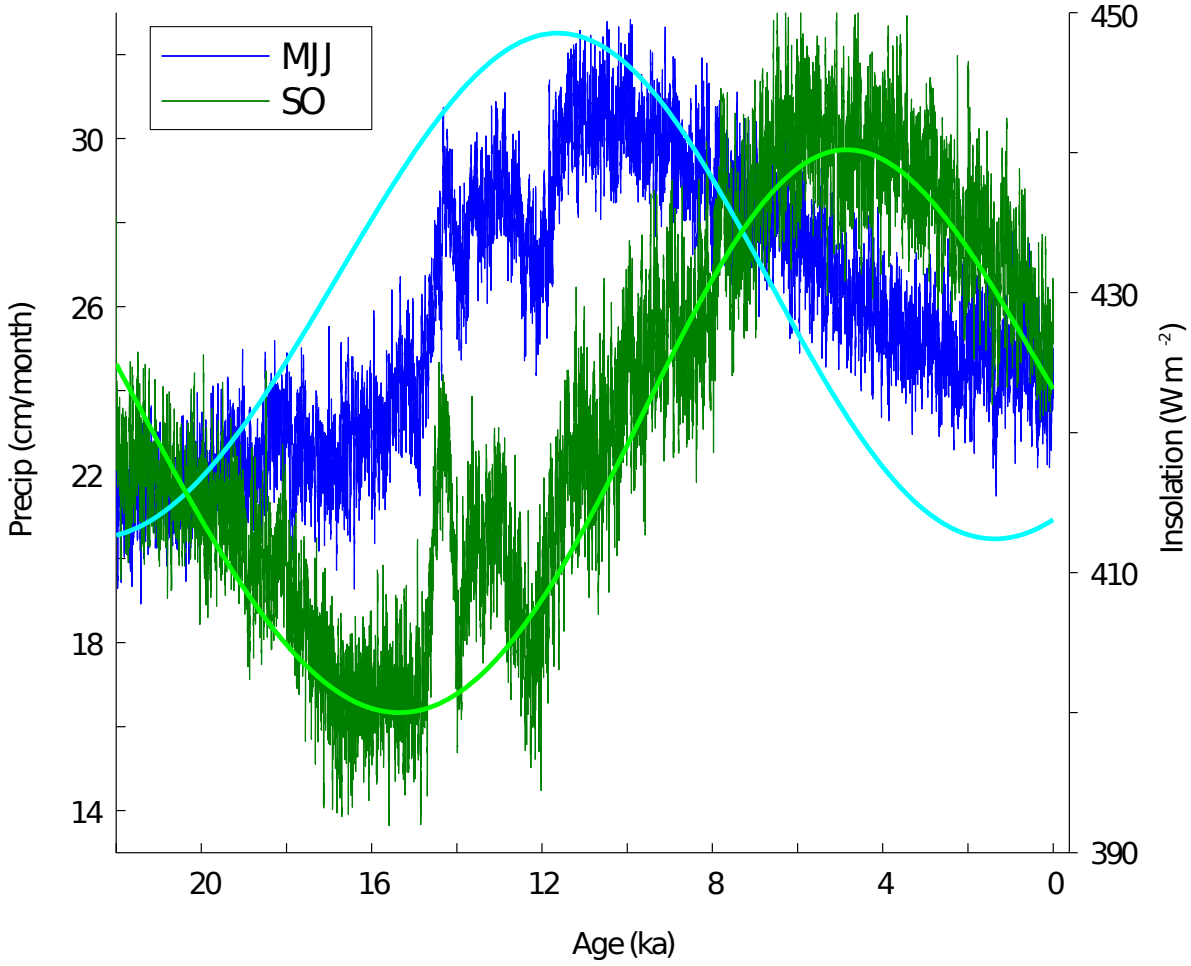

Figure S11. Differences in monthly precipitation variability driven by changing insolation over the Holocene. Simulated seasonal precipitation and insolation at the Lake Bosumtwi over the past 22,000 years. Mean monthly precipitation for May, June and July are shown in blue, and mean monthly precipitation for September and October are shown in green. Both precipitation curves are smoothed with an 11-year running mean. Seasonal mean insolation at 6.5°N for the corresponding months are shown in cyan and bright green.

The time-transgressive termination of the African Humid Period

Timothy M. Shanahan, Nicholas P. McKay, Konrad A. Hughen, Jonathan T. Overpeck, Bette Otto-Bliesner, Clifford W. Heil, John King, Christopher A. Scholz, John Peck

Supplementary Table

Table S1. Locations of paleohydrological sites across North Africa.

number	site	location	lat	lon	proxy	reference
1	Sebkha mellala	Algeria	32.18	5.20	1,2	27,35-37
2	Hassi el Mejnah	Algeria	31.67	2.50	1,2,3	27,36,38,39
3	GeoB5546	Atlantic	27.54	-13.74	4	40
4	OC437-7 GC37	Atlantic	26.82	-15.12	4	41
5	OC437-7 GC49	Atlantic	23.21	-17.85	4	41
6	ODP 658C	Cape Blanc	20.75	-18.58	4	42
7	OC437-7 GC68	Atlantic	19.36	-17.28	4	41
8	GeoB9508-5	Senegal	15.50	-17.95	5,7	32,43
9	Diogo	Senegal	15.26	-16.80	6	44
10	Erg Akchar	Mauritania	21.98	-13.32	2	27,45,46
11	Chemchane	Mauritania	20.93	-12.22	7	27,47-49
12	Agorgott	Mali	22.65	-4.02	2	27,50-52
13	Wadi Haijad	Mali	22.57	-3.67	1,2,3	27,36,53,54
14	Tagnout-Chaggaret	Mali	21.22	-0.68	2	27,53
15	Ine Kousamene	Mali	20.60	-0.85	2	27,53
16	Agneby	Ivory Coast	5.33	-4.25	6	126
17	Ounjougou	Mali	14.60	-3.07	2	56
18	Oursi	Burkina Faso	14.65	-0.13	6	57
19	erg Uan Kasa	Libya	25.76	10.89	2,3	58,59
20	Tadrart Acacus	Libya	10.50	25.50	2	
21	Adrar Bous	Niger	20.29	9.01	1,2,3	27,35,36
22	Tin Ouaffadene	Niger	20.18	9.19	1,2,4	27,35,36
23	Fachi	Niger	18.10	11.30	2	27,60,61

24	Dibella	Niger	17.53	13.13	2	62
25	Kawar	Niger	18.60	13.08	2,3	27,60,61
26	Termit	Niger	16.00	11.25	2,3,7	36,63
27	Jikariya Lake	Nigeria	13.31	11.08	6	64
28	Bougdouma	Niger	13.32	11.67	2,3	35,36
29	Kaigama	Nigeria	13.25	11.56	6	65
30	Kajemarum	Nigeria	13.30	11.02	2,7	27,36,65-67
31	Komadugo	Nigeria	12.83	12.00	2	68
32	Bal lake	Nigeria	13.31	10.95	6	27,65
33	Wadi Fesh Fesh	Sudan	18.90	17.90	2,3,7	27,69-72
34	Bahr el Ghazal	Chad	15.42	18.02	2	73,74
35	Yoa	Chad	19.03	20.31	2,6	75,76
36	Farafra	Egypt	27.10	28.10	2	77-79
37	Dakhla oasis	Egypt	25.23	29.42	2	80,81
38	Selima Oasis	Sudan	20.92	27.68	2,3	27,71,82-86
39	Dry Selima	Sudan	21.37	29.17	1,2,3	27,69,84,87,88
40	Oyo	Sudan	19.27	26.18	2,6	27,82,83,89
41	Lake Gureinat	Sudan	16.97	27.30	1,7	90
42	Meidob Hills	Sudan	15.35	26.35	2,7	27,84,91
43	Atrun	Sudan	18.17	26.15	6	27,71,72,83
44	ridge lake T175	Sudan	16.60	27.63	2,3	27,71,72
45	Wadi Howar	Sudan	17.60	27.50	2,6	27,71,72,92,93
46	Wadi Mansurab	Sudan	15.42	32.22	1,2	94,95
47	Rukwa	Tanzania	8.42	32.75	3	97
48	Massoko	Tanzania	9.33	33.75	3	98
49	Tana	Ethiopia	12.00	37.25	5	99
50	Abhe	Ethiopia	11.10	41.40	2,3	100,101
51	Abiyata	Ethiopia	7.30	38.40	3	102
52	P178-15P	Gulf of Aden	11.96	44.30	5	103
53	NIOP 905	Arabian Sea	50.00	10.00	4	104
54	Ziway-Shalla	Ethiopia	7.50	38.40	2	105-107
55	Tilo	Ethiopia	7.06	38.09	1	108
56	Kuruyange	Burundi	3.83	29.68	6	109
57	Rusaka	Burundi	3.43	29.62	6,7	110,111
58	Muchoya	Uganda	1.28	29.80	6	112
59	Edward	Uganda	-0.42	29.58	3,6,7	113
60	Turkana	Kenya	2.67	36.50	2,3	114
61	Victoria	Tanzania	1.00	33.00	1,3	115,116
62	Mt Satima Mire	Kenya	0.30	36.58	7	117
63	Challa	Tanzania	-3.32	37.70	5	18
64	Tanganyika	Tanzania	-6.70	29.83	5	118
65	Cheshi	Zambia	-9.08	29.75	3	119
66	Tilla	Nigeria	10.38	12.13	1,2,3	120,121
67	Segedim	Niger	10.17	12.78	6	27,60,122
68	Bosumtwi	Ghana	6.50	-1.42	2,5	this paper
69	Sélé	Benin	7.15	2.43	6	123
70	Dangbo	Benin	6.61	2.60	6	124
71	Dogla	Benin	6.53	2.37	6	124
72	Yeviedie	Benin	6.53	2.38	6	124

73	Lac Nokoue	Benin	6.50	2.39	6	124
74	Goho	Benin	6.44	2.58	6	124
75	Badagry	Niger	6.43	2.77	6	125
76	Bilanko	Congo	15.35	-3.52	6	55
77	Barombi Mbo	W Africa	4.67	9.40	6,7	127-129
78	MD03-2707	GOG	2.50	9.39	1,3,7	130
79	Njupi	Cameroon	6.45	10.32	6	131-133
80	Shum Laka	Cameroon	5.85	10.05	6	134,135
81	Bafounda Swamp	Cameroon	5.53	10.33	6	131,136
82	Mbalang	Cameroon	7.32	13.73	6	137,138
83	Ossa	Cameroon	3.80	10.75	6,7	139,140
84	Nyabessan	Cameroon	2.67	10.67	6	141
85	Lake Goualougo	Congo	2.16	16.51	6	142
86	Mopo Bai	Congo	2.24	16.93	6	143
87	Lake Tele	Congo	1.33	17.17	6	144
88	Lake Maridor	Gabon	-0.17	9.35	6	131,132,145
89	Lake Nguene	Gabon	-0.20	10.47	6	131,132,145
90	Lake Kamalete	Gabon	-0.72	11.77	6	131,132,145
91	Congo	GOG	-5.58	11.22	5	31
92	Coraf	Congo	-4.75	11.85	6	131,132,146
93	Kitina	Congo	-4.25	11.98	6	131,132,147
94	Sinnda	Congo	-3.84	12.80	6	132,148
95	Songolo	Congo	-4.76	11.86	6,7	131,132,149
96	Ngamakala	Congo	-4.07	15.38	6	146,150

Proxy types: 1- oxygen isotopes, 2- stratigraphy/lithology, 3- biological indicators, 4- terrigenous fluxes, 5- δD_{wax}, 6- pollen, 7- geochemistry